ANALYSIS OF HIGH-ORDER SPECTRAL INTERPOLATION APPLIED TO 2D ELASTOSTATIC BEM

Renério Pereira Neto

Fabio Carlos da Rocha

rneto@academico.ufs.br

fcrocha@ufs.br

Department of Civil Engineering. Federal University of Sergipe.

Av. Marechal Rondon, s / n, 49100-000, São Cristóvão, SE, Brazil.

Aref Kalilo Lima Kzam

aref.kzam@unila.edu.br

Abstract. *In the direct formulation of the boundary element method, significant numerical errors can occur when trying to reproduce a complex physical fields accurately. The polynomial interpolation and the order of the approximations employed influence these errors, which affect the physical solution of the problem. This work presents a comparative study between the equidistant nodes approach and the spectral base applied in the analysis of two-dimensional elastostatic problems by boundary element method. High order approximations are used to verify the method's conditioning. Based on the evaluation of the Lebesgue constant, a convergence analysis is carried out by means the high order polynomials error caused by Runge phenomenon. Examples are evaluated and improvements of the results are verified by using a spectral interpolation.*

Keywords: *Equidistant base, spectral base, Runge phenomenon, Lebesgue constant.*

Proceedings of the XXXVIII Iberian Latin-American Congress on Computational Methods in Engineering P.O. Faria, R.H. Lopez, L.F.F. Miguel, W.J.S. Gomes, M. Noronha (Editores), ABMEC, Florianópolis, SC, Brazil, November 5-8, 2017.

1 INTRODUCTION

A few decades ago the numerical modeling has been taking more space in the technical and academic community to solve large and complex physical problems. Moreover, among numeric methods, accurate and efficient, used in the computer simulation it highlights the Boundary Element Method (BEM).

The boundary element method (BEM) is generally employed using approaches with lower order elements, wherein the solution of the integral equation is approximated by constant, linear or quadratic functions in each element (Brebbia, 1978; Pozrikidis, 1992). However, due to the low accuracy in describing both complex geometries and/or various physical problems, the use higher order elements has been recommended (Karniadakis, Sherwin, 1999), instead of low-order approximations.

As an alternative to high-order elements with evenly spaced basis, this work analyzes the spectral approximation of higher order, which makes use of the basic nodal of Lobatto. In this spectral approach, the interpolation points, or collocation points for the BEM, are positioned in the zeros of the orthogonal polynomial of Lobatto.

To verify the performance of two nodal base sets along a curve, both the condition number of the generalized Vandermond matrix and Lebesgue constant are used. This last parameter is defined as the maximum value of the absolute sum of the interpolation function on all nodes. These two parameters are important quantifiers of the high-order polynomial interpolation error due to the possibility of occurrence of the oscillatory phenomenon called Runge (Chen, He, Zhang, 2013)

In this work the two-dimensional elatostatic BEM is used, where the collocation points are applied in the zeros of Lobatto polynomials and the results are compared with conventional collocation points (evenly spaced) for convergence as the degree of approximation is increased.

The paper is organized as follows: Section 2 is intended for the presentation of the BEM elastostatics problems. Section 3 presents the high order interpolations, item 3.1 shows the equidistant nodal basis and in item 3.2 shows the spectral interpolation and a nodal base Lobatto. Section 3.3 addresses for conditioning of the matrix and Vandermond generalized interpolation error by studying convergence and Lebesgue constant. In the following topics, examples are presented to illustrate the results of the method.

2 BEM FOR 2-D ELASTOSTATIC PROBLEMS

There are several ways to get the formulations of boundary element method (BEM), such as by Betti's reciprocity theorem, by the concepts of the weighted residuals and the variational approach. The BEM formulation for two-dimensional elastostatic problems with source point belonging to the domain Ω is given by (Aliabadi, 2002):

$$\boldsymbol{u}(x') + \int_{\Gamma} \boldsymbol{T}(x', x).\boldsymbol{u}(x)\, d\Gamma = \int_{\Gamma} \boldsymbol{U}(x', x).\boldsymbol{t}(x)\, d\Gamma + \int_{\Omega} \boldsymbol{U}(x', X).\boldsymbol{b}(X)\, d\Omega. \quad (1)$$

In that $\boldsymbol{u}$, $\boldsymbol{t}$ and $\boldsymbol{b}$ are the displacement, tractions and body forces, respectively. The points x and X represent field values on the boundary and in the domain problem, respectively. Already, the point x' is the source point belonging to the domain Ω. In this work the tensor notation is used $(a \otimes b \otimes c)^{321} = (c \otimes b \otimes a)$, such that $\boldsymbol{D}^{312} = D_{kij}(\boldsymbol{e}_i \otimes \boldsymbol{e}_j \otimes \boldsymbol{e}_k)$ e $\boldsymbol{S}^{312} = S_{kij}(\boldsymbol{e}_i \otimes \boldsymbol{e}_j \otimes \boldsymbol{e}_k)$.

The Eq. (1) applied to the constitutive law obtains the integral identity for stress as follows:

$$\boldsymbol{\sigma}(x') + \int_{\Gamma} \boldsymbol{S}^{\boldsymbol{312}}(x', x).\boldsymbol{u}(x)\, d\Gamma = \int_{\Gamma} \boldsymbol{D}^{\boldsymbol{312}}(x', x).\boldsymbol{t}(x)\, d\Gamma + \int_{\Omega} \boldsymbol{D}^{\boldsymbol{312}}(x', X).\boldsymbol{b}(X)\, d\Omega. \quad (2)$$

The fundamental solutions are described by (Aliabadi, 2002):

$$\boldsymbol{U}(x', x) = \frac{1}{8\pi G(1-\nu)}\left((3-4\nu)\ln\left(\frac{1}{r}\right)\boldsymbol{I} + \hat{\boldsymbol{r}} \otimes \hat{\boldsymbol{r}}\right); \quad (3)$$

$$\boldsymbol{T}(x', x) = \frac{-1}{4\pi(1-\nu)r}\{(\boldsymbol{n}.\nabla r)[(1-2\nu)\boldsymbol{I} + 2\hat{\boldsymbol{r}} \otimes \hat{\boldsymbol{r}}] + (1-2\nu)(\boldsymbol{n} \otimes \hat{\boldsymbol{r}} - \hat{\boldsymbol{r}} \otimes \boldsymbol{n})\}; \quad (4)$$

$$\boldsymbol{D}^{\boldsymbol{312}}(x', x) = \frac{1}{4\pi(1-\nu)r}\{(1-2\nu)[(\boldsymbol{I} \otimes \hat{\boldsymbol{r}}) + (\boldsymbol{I} \otimes \hat{\boldsymbol{r}})^{\boldsymbol{132}} - (\hat{\boldsymbol{r}} \otimes \boldsymbol{I})] + 2\hat{\boldsymbol{r}} \otimes \hat{\boldsymbol{r}} \otimes \hat{\boldsymbol{r}}\}; \quad (5)$$

$$\boldsymbol{S}^{\boldsymbol{312}}(x', x) = \frac{\mathrm{G}}{2\pi(1-\nu)r^2}\begin{Bmatrix} 2(\boldsymbol{n}.\hat{\boldsymbol{r}})\begin{bmatrix}(1-2\nu)\hat{\boldsymbol{r}} \otimes \boldsymbol{I} + \\ \nu[(\boldsymbol{I} \otimes \hat{\boldsymbol{r}})^{\boldsymbol{213}} + (\boldsymbol{I} \otimes \hat{\boldsymbol{r}})^{\boldsymbol{312}}] - 4\hat{\boldsymbol{r}} \otimes \hat{\boldsymbol{r}} \otimes \hat{\boldsymbol{r}}\end{bmatrix} + \\ 2\nu(\hat{\boldsymbol{r}} \otimes \boldsymbol{n} \otimes \hat{\boldsymbol{r}} + \hat{\boldsymbol{r}} \otimes \hat{\boldsymbol{r}} \otimes \boldsymbol{n}) - (1-4\nu)\boldsymbol{n} \otimes \boldsymbol{I} + \\ (1-2\nu)[2\boldsymbol{n} \otimes \hat{\boldsymbol{r}} \otimes \hat{\boldsymbol{r}} + (\boldsymbol{I} \otimes \boldsymbol{n})^{\boldsymbol{213}} + (\boldsymbol{I} \otimes \boldsymbol{n})^{\boldsymbol{312}}] \end{Bmatrix}; \quad (6)$$

where $r_i = x_i - x'_i$, $r = (r_i r_i)^{1/2}$, $\hat{\boldsymbol{r}} = r_i/r$.

The boundary integral equations for displacements (Eq. 1) and stress (Eq. 2) is valid for any source point within the domain Ω. In order to obtain the solution to the point on boundary, it is necessary to consider the limit when $x' \to x$, with $x \in \Gamma$. The process is carried out by considering a semi-circular region surrounding the point source x', such that the new contour region, Γ^A, is given by

$$\Gamma^A = (\Gamma - \Gamma_\epsilon) + \Gamma_\epsilon^+. \quad (7)$$

Where Γ_ϵ is portion of the original contour removed, and Γ_ϵ^+ is portion inserted to this contour. The behavior of the singularities is studied considering the limit $\epsilon \to 0$ and therefore $\Gamma^A \to \Gamma$. Thus, by performing limit analysis, one can write (Aliabadi, 2002):

$$\boldsymbol{C}(x').\boldsymbol{u}(x') + \lim_{\epsilon \to 0}\left\{\int_{\Gamma-\Gamma_\epsilon}[\boldsymbol{T}(x', x).\boldsymbol{u}(x) - \boldsymbol{U}(x', x).\boldsymbol{t}(x)]\, d\Gamma\right\} = \int_{\Omega} \boldsymbol{U}(x', X).\boldsymbol{b}(X)\, d\Omega; \quad (8)$$

$$\overline{\boldsymbol{C}}(x'):\boldsymbol{\sigma}(x') + \lim_{\epsilon \to 0}\left\{\int_{\Gamma-\Gamma_\epsilon}\left[\boldsymbol{S}^{\boldsymbol{312}}(x', x).\boldsymbol{u}(x) - \boldsymbol{D}^{\boldsymbol{312}}(x', x).\boldsymbol{t}(x) + \boldsymbol{u}(x').\frac{\boldsymbol{B}^{312}(x')}{\epsilon}\right] d\Gamma\right\} = \int_{\Omega} \boldsymbol{D}^{\boldsymbol{312}}(x', X).\boldsymbol{b}(X)\, d\Omega. \quad (9)$$

where the tensor $\boldsymbol{C}(x')$, $\overline{\boldsymbol{C}}(x')$ and $\boldsymbol{B}^{312}(x')$ are coefficients (limited) that depend only the local geometry Γ only x'. If x' is a smooth boundary point and Γ_ϵ has circle shape, the free term $\boldsymbol{C}(x')$ and $\overline{\boldsymbol{C}}(x')$ in Eqs. (8) and (9) are reduced $0{,}5\boldsymbol{I}$ and $0{,}5\overline{\boldsymbol{I}}(= 0{,}5\delta_{ij}\delta_{th})$.

The singularity level of kernel of the boundary integral equations in Eqs. (1) and (2) can be defined as (Gao, 2010)

$$\begin{cases} \beta \leq 0, \ Regular \\ 0 < \beta \leq D-1, \ Weakly\ singularity \\ \beta = D-1, \ Strongly\ singularity \\ \beta = D, \ Hypersingular \\ \beta > D, \ Supersingular \end{cases} \tag{10}$$

where $D$is Cartesian dimension (in this work $D = 2$) and β is the exponent accompanying the distance between the field point and the point source, $f(x', x)/r^{\beta}$. Thus, according to Eq. (10), the Eq. (3) is classified as regular, the Eq. (4) and (5) are strongly singular and Eq. (6) hyper-singular.

The BEM methodology consist of numerically solving the wee-posed contour value problem, which is constituted by the system of integral equation provided by Eq. (1). For this purpose and neglecting body forces, the smooth surface Γ is discretized in curved boundary element E of any order. To a nodal point k, on the boundary, Eq (1) have, respectively, form:

$$\frac{\mathbf{1}}{\mathbf{2}}\boldsymbol{u}\left(x'^{k}\right) + \sum_{e=1}^{E}\sum_{a=1}^{A(e)}\int_{-1}^{1}\boldsymbol{T}\left(x'^{k}, x(\varepsilon)\right)\varphi^{a}(\varepsilon)J(\varepsilon)d\varepsilon\,.\,u_a^e = \sum_{e=1}^{E}\sum_{a=1}^{A(e)}\int_{-1}^{1}\boldsymbol{U}\left(x'^{k}, x(\varepsilon)\right)\varphi^{a}(\varepsilon)J(\varepsilon)d\varepsilon\,.\,t_a^e\,; \tag{11}$$

With $A(e)$ the number of nodes of the element e, φ^a are the functions of one-dimensional shape of a curved element, J the Jacobian of the transformation of the global coordinate system (X_1, X_2) for dimensionless local coordinate (ε) and, finally, u_a^e and t_a^e are the nodal values of the corresponding field functions. For simplicity, global numbering is used for the nodes, that is, each pair (e, a) is associated with a number β. Thus, the Eq. (11) is rewritten in a discrete form:

$$\frac{\mathbf{1}}{\mathbf{2}}\boldsymbol{u^k} + \sum_{\beta=1}^{L} H_{\beta}^{k}.u^{\beta} = \sum_{\beta=1}^{L} G_{\beta}^{k}.t^{\beta}, \tag{12}$$

where L is the total number of nodes and

$$H_{\beta}^{k} = \int_{-1}^{1}\boldsymbol{T}\left(x'^{k}, x(\varepsilon)\right)\varphi^{a}(\varepsilon)J(\varepsilon)d\varepsilon, \tag{13}$$

$$G_{\beta}^{k} = \int_{-1}^{1}\boldsymbol{U}\left(x'^{k}, x(\varepsilon)\right)\varphi^{a}(\varepsilon)J(\varepsilon)d\varepsilon. \tag{14}$$

Applying the boundary conditions, displacement and traction prescribed to Eq. (12) it is possible to write the final linear system in the form

$$\boldsymbol{A\,X} = \boldsymbol{B}, \tag{15}$$

in that the vectors $\boldsymbol{X}$ and $\boldsymbol{B}$ contain all the unknowns and prescribed values of the nodal components of boundary, respectively.

Similarly, the discrete equation is written into the domain stress field as follows

$$\boldsymbol{\sigma^i} + \sum_{\beta=1}^{L}\bar{H}_{\beta}^{k}.u^{\beta} = \sum_{\beta=1}^{L}\bar{G}_{\beta}^{k}.t^{\beta}\,; \tag{16}$$

with

$$\bar{H}_{\beta}^{k} = \int_{-1}^{1} \boldsymbol{S^{312}}\left(x'^{k}, x(\varepsilon)\right) \varphi^{a}(\varepsilon) J(\varepsilon) d\varepsilon, \tag{17}$$

$$\bar{G}_{\beta}^{k} = \int_{-1}^{1} \boldsymbol{D^{312}}\left(x'^{k}, x(\varepsilon)\right) \varphi^{a}(\varepsilon) J(\varepsilon) d\varepsilon. \tag{18}$$

3 POLYNOMIAL INTERPOLATION

Among numerous methods to obtain the interpolating polynomials, can be mentioned, the generation from the Vandermond generalized matrix. For this methodology, it is considered a dimensionless coordinate basis, generated from a set of points {ξk ∈ ℝ; -1 ≤ 1 ≤ ξk} depend on the degree of approximation. The general term of the polynomial is shown in Eq. (19), where φ_i are the shape functions with m degree evaluated in points given by Eq. (20) (Rocha; Kzam; Coda, 2013).

$$P_m(x) = \sum_{i=1}^{m+1} f_i(x) \varphi_i(\xi) \tag{19}$$

$$\varphi_i(\xi) = \sum_{j=0}^{m} a_{ij} \xi^{j} = a_{i0} + a_{i1}\xi + \cdots + a_{im}\xi^{m} \tag{20}$$

From the imposition of the Delta Kronecker property, Eq. (20) can be rewritten in the form:

$$\varphi_i(\xi = \xi_k) = a_{i0} + a_{i1}\xi_k + \cdots + a_{im}{\xi_k}^{m} = \delta_{ik} \tag{21}$$

In matrix notation, the Eq. (21) can be written:

$$\begin{bmatrix} a_{10} & a_{11} & \cdots & a_{1m} \\ a_{20} & a_{21} & \cdots & a_{1m} \\ \vdots & \vdots & \ddots & \vdots \\ a_{k0} & a_{k1} & \cdots & a_{km} \end{bmatrix} \begin{bmatrix} 1 & 1 & \cdots & 1 \\ \xi_1 & \xi_2 & \cdots & \xi_k \\ \vdots & \vdots & \ddots & \vdots \\ \xi_1^m & \xi_2^m & \cdots & \xi_k^m \end{bmatrix} = \begin{bmatrix} 1 & 0 & \cdots & 0 \\ 0 & 1 & \cdots & 0 \\ \vdots & \vdots & \ddots & \vdots \\ 0 & 0 & \cdots & 1 \end{bmatrix} \tag{22}$$

The matrix with the powers of the generalized dimensionless coordinates is called Generalized Vandermond matrix, whose inverse given the coefficients a_{ij}.

Among the different ways of determining the set of dimensionless nodes ξk, this work was made use of evenly spaced nodal base and Lobatto nodal base for high-order approximations.

3.1 Evenly spaced nodal Base

To determine m + 1 equally spaced nodes, in the dimensionless space, dependent of the degree m of approximation, can make use of the general term of the arithmetic progression, below (Rocha; Kzam; Coda, 2013):

$$\xi_k = \xi_1 + (k-1)r \tag{23}$$

being the ratio progression r defined as $r = \frac{2}{m}$, $\xi_1 = -1$ and k = 1, 2, ..., (m + 1).

3.2 Spectral interpolation and Lobatto's nodal base

The spectral interpolation method, the interpolation nodes are placed in the zeros of orthogonal polynomials belonging to the dimensionless space {ξk ∈ ℝ; -1 ≤ ξk ≤ 1}, subject to the constraint that ξ1 = -1 and ξm + 1 = 1, and m, the degree of the polynomial approximation, with m +1 nodes.

For the spectral convergence, a way to improve accuracy is given by increasing the interpolation order. Thus, the error decreases at a rate that is faster than any power 1/ m, and m the order polynomial expansion. This type of convergence is rated refinement - p (Pozrikidis, 2005).

Consider a family of polynomials $\phi_0(x)$, $\phi_1(x)$, $\phi_2(x)$, ... with 0, 1, 2, ... the degrees. The polynomials $\phi_0(x)$, $\phi_1(x)$, $\phi_2(x)$, ... are orthogonal and satisfy the scalar product defined by Eq. (24), i.e. the polynomials are perpendicular to each other. The weighting function $\omega(x)$ should be continuous on the interval [a, b], and $\omega(x) \geq 0$ (Franco, 2006).

$$\left(P_i, P_j\right) = \int_a^b P_i(x)P_j(x)\omega(x)dx = \begin{cases} 0, for\ i \neq j \\ \alpha \neq 0, for\ i = j \end{cases} \tag{24}$$

The Eq. (24) can be rewritten as follows, from the imposition of the Kronecker property:

$$\left(P_i, P_j\right) = \int_a^b P_i(x)P_j(x)\omega(x)dx = \alpha\delta_{ij} \tag{25}$$

From the spectral interpolation theory, the node ends (ξ_1 = -1 e ξ_{m+1} = 1) must be fixed and the m – 1 remaining nodes must be located at the zeros of certain polynomials that obey Eq. (25). Thus, the polynomial of Lobatto satisfies the following property (Pozrikidis, 2005):

$$\int_{-1}^{1} Lo_i(\xi)Lo_j(\xi)(1-\xi^2)d\xi = \begin{cases} 0, for\ i \neq j \\ \frac{2(i+1)(i+2)}{2i+3}, for\ i = j \end{cases} \tag{26}$$

The Lobatto polynomial of degree m, is derived from Legendre polynomial of degree m + 1.

$$Lo_m(\xi) = L'_{m+1}(\xi) \tag{27}$$

The first terms and recurrence function of the Lobatto polynomial are shown in Table 1. In the Fig. 1 the behavior of the Lobatto polynomial with degree varying from 1 to 4 is shown.

Table 1. Lobatto Polynomials: Recurrence ratio

$Lo_0(\xi) = 1$ $Lo_1(\xi) = 3\xi$ $Lo_2(\xi) = \frac{3}{2}(5\xi^2 - 1)$ $Lo_3(\xi) = \frac{5}{2}(7\xi^2 - 3)\xi$	$Lo_4(\xi) = \frac{15}{8}(21\xi^4 - 14\xi^2 + 1)$ ⋮ $Lo_m(\xi) = \frac{1}{\xi^2-1}[(m+1)\xi L_{m+1}(\xi) - (m+1)L_m(\xi)]$

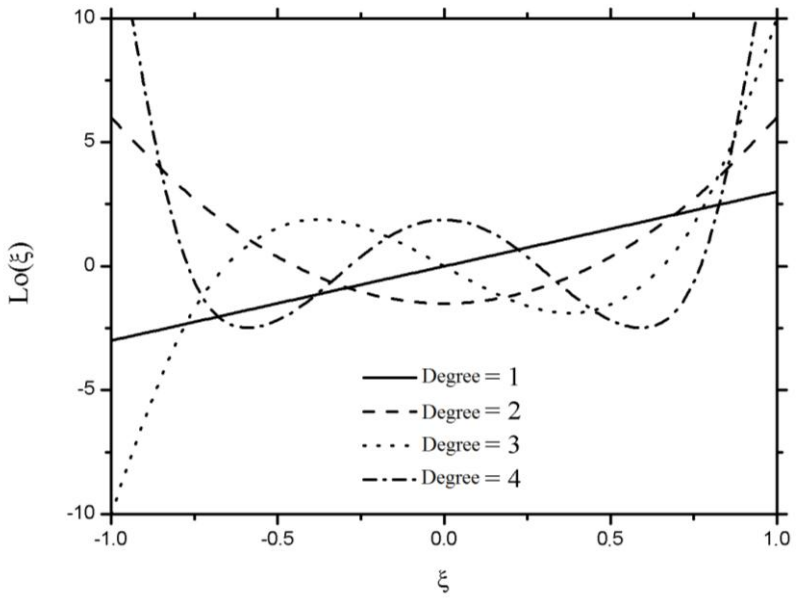

Figure 1. First terms of Lobatto polynomials.

3.3 Condition number and Lesbegue constant.

A problem is said to be well conditioned when large perturbations in the data cause small disturbance in the linear system solution. On the contrary, when small perturbations in the data cause major perturbations in the results, it is said that this is an ill-conditioned problem. One way to quantify this feature is given by the analysis of the condition number. Thus, as lower the condition number as better the conditioning of the problem (Franco, 2006).

The condition number of the matrix A is defined as:

$$cond(A) = \|A\|\|A^{-1}\| \tag{28}$$

Once the inverse matrix of any order is defined, it is possible to calculate its norm and, consequently, the norm of its inverse, by Euclidian norm defined by:

$$\|A\|_E = \sqrt{\sum_{i,j=1}^{m} a_{ij}^2} \tag{29}$$

Thus, this study aimed to evaluate the conditioning of the Vandermonde matrix to different bases of approximation. The condition number for the bases equidistant and Lobatto is shown in Figure 2 as the degree of approximation is increased. It is also observed, in Fig. (2), the greatest ill-conditioning when used evenly spaced based on comparison with the Lobatto nodal points.

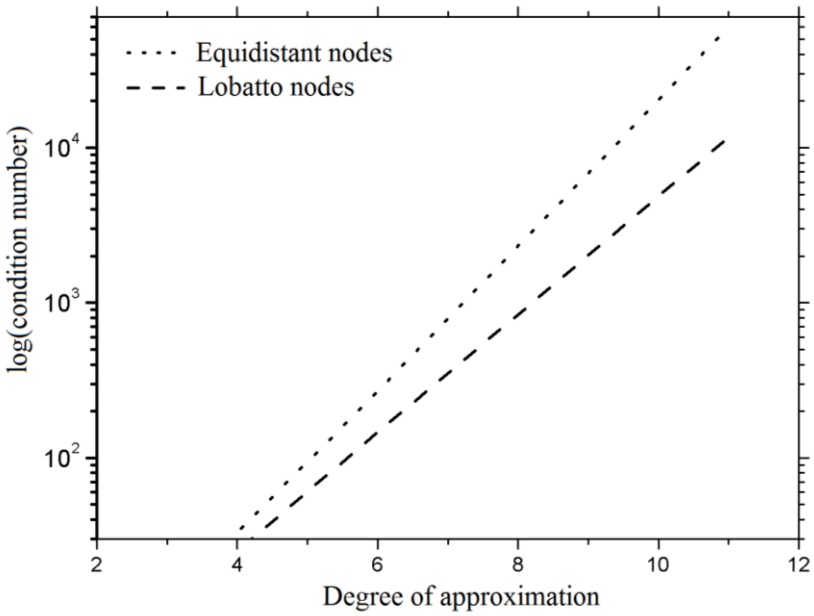

Figure 2. Condition number for the Vandermonde matrix

The quantification of the performance of the studied bases is done through the Lesbegue constant (Eq. 31), which is defined from the Lebesgue function (Eq. 30) (Pozrikidis, 2005).

$$\Im_m(\xi) \equiv \sum_{i=1}^{m+1} |\varphi_i(\xi)| \tag{30}$$

$$\Lambda_m \equiv Max(\Im_m(\xi)) \tag{31}$$

Thus, the Lebesgue constant can be understood as the maximum absolute value of the sum of shape functions applied at any dimensionless points, ξ_k , belonging to the interval [-1 ≤ ξ_k ≤ 1]. Therefore, the base that have lower value for this constant, provide lower interpolation error.

To illustrate the influence of bases studied here, was considered the function of Eq. (32), which should be approximated and measured convergence when increasing the order of the interpolation. It is possible to realize, with the aid of Fig. (3), that the base of evenly spaced nodes deteriorates more rapidly compared to the Lobatto nodal base, as the degree of approximation increases. In both Fig. 4 e Tab. 2 respectively, the behavior of the Lebesgue constant is presented, qualitatively and quantitatively, as the degree of approximation varies. It can be observed (see Fig. 4 and Tab. 2) that the equidistant base presents unlimited values compared to the Lobatto base for the Lebesgue constant, which may provide better interpolation for the latter base.

$$f(x) = \frac{1}{1+25x^2} \tag{32}$$

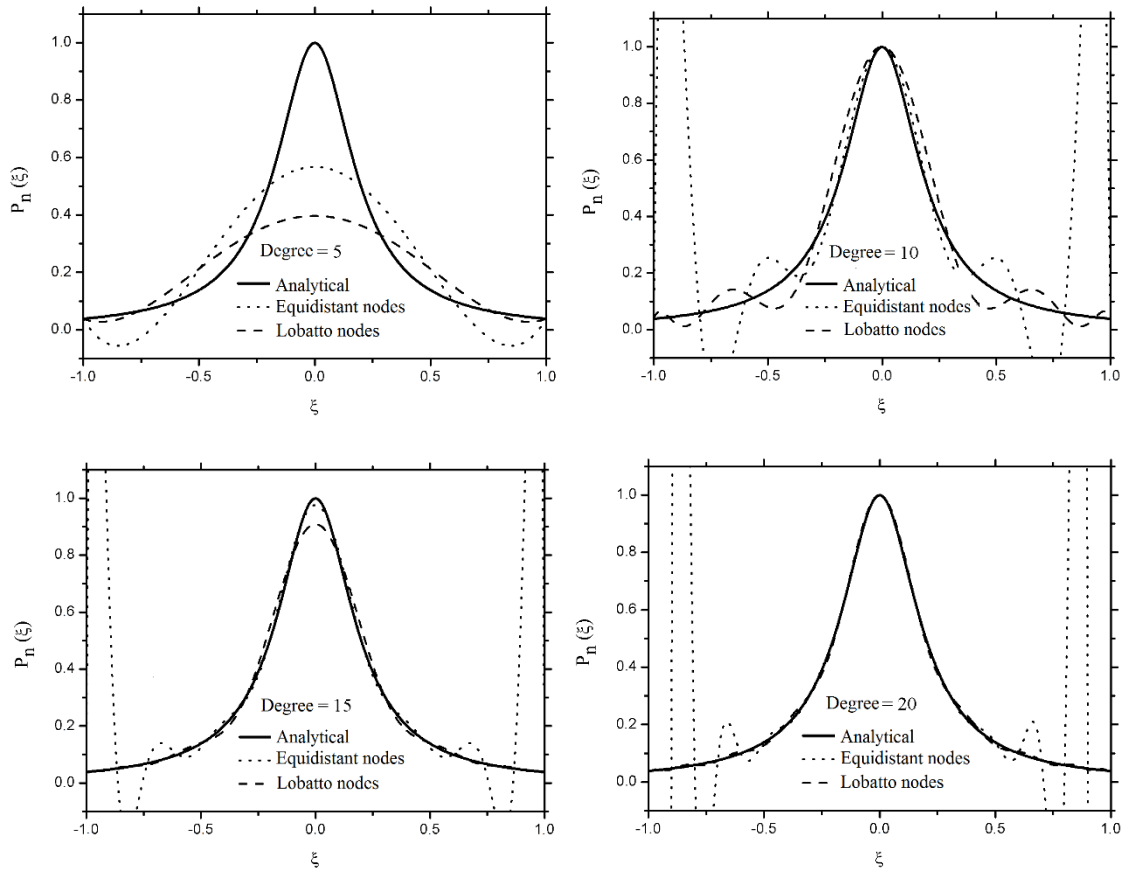

Figure 3. Approximation of rational function by evenly spaced and Lobatto nodes

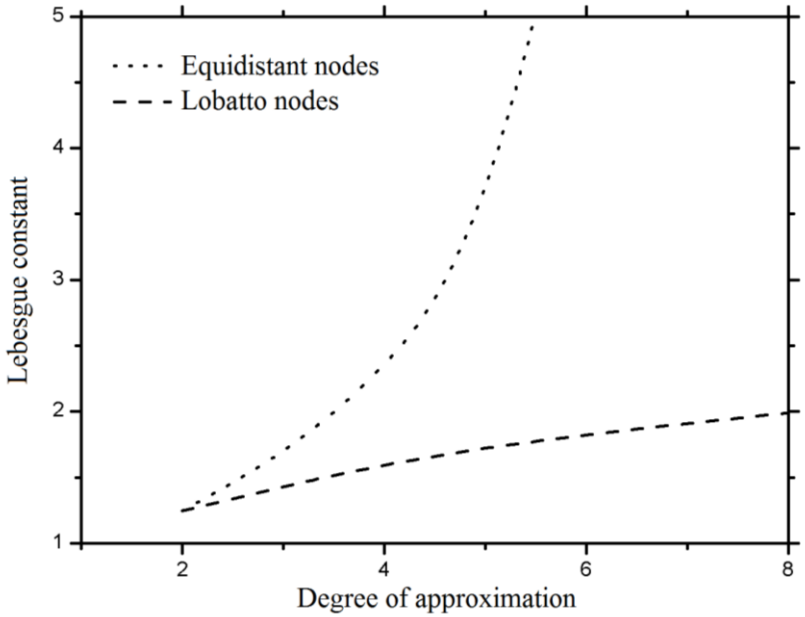

Figure 4. Lebesgue constant for nodal bases

Table 2. Lebesgue constant for various degrees of interpolation

Order	Equidistant nodes	Lobatto nodes
2	1.24997	1.24997
4	2.20703	1.63567
6	4.54926	1.87291
8	10.94178	2.04333
10	29.89705	2.18020
15	508.35160	2.41384
20	10714.42407	2.59551

4 APPLICATION

The interpolation strategies are applied to the Boundary Element Method. The objective is to evaluate the influence of nodal bases in the representation of the physical response of two-dimensional elastostatic problems. Therefore, it was taken as example (see Fig. 4), a pressurized

cylinder with the following data: inner radius (r_i) of 10 cm, external radius (r_o) of 20 cm, internal pressure (P) of 10 MPa, modulus of elasticity (E) 210 GPa and Poison coefficient (ν) 0,3.

Due to the symmetry in both geometry as loading, the analysis was simplified to a quadrant of cylinder, as shown in Fig. (5). In order to measure the potential of the method as well as the influence of nodal basis, it is adopted the analytical solution, in strain plane state, for both displacement (Eq. 33) and to stress (Eq. 34) in radial direction, as the reference result.

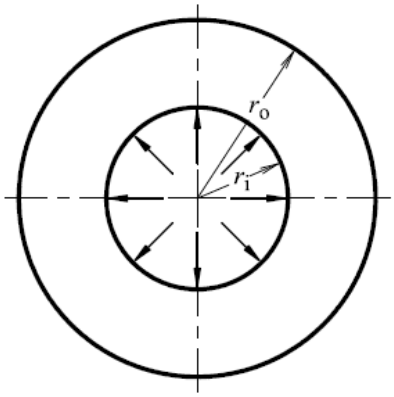

Figure 4. Pressurized cylinder

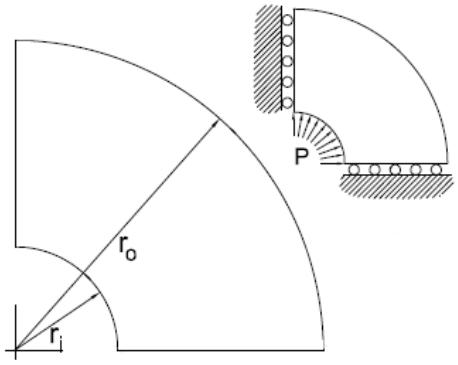

Figure 5. Simplified Analysis

$$u_r = \frac{(1+\nu)Pr}{E\left[\left(\frac{r_o}{r_i}\right)^2 - 1\right]}\left[\left(\frac{r_o}{r}\right)^2 + (1-2\nu)\right] \tag{33}$$

$$\sigma_r = \frac{Pr_i{}^2}{r_o{}^2 - r_i{}^2}\left[1 - \left(\frac{r_o}{r}\right)^2\right] \tag{34}$$

In numerical analysis by BEM they were adopted four elements with a degree of approximation ranging from 5 to 20. From this variation is possible to evaluate the influence of node bases the mechanical response of the proposed problem.

In Fig. (6) the variation of the radial displacement is shown for the points, on boundary, obtained by both the reference solution as BEM, as the order of approximation is high. A strong

oscillation is also observed when the reference solution is approached using the equidistant nodal base. On the other hand, for physical response obtained by use of Lobatto nodal base is verified both stability as the excellent agreement of the response, with the analytical solution.

The instability in the physical response of the contour, due to the equally spaced base approximation inserts significant errors in the analysis of the internal displacement field, as can be seen in Fig. (7). However, when the Lobatto base is used, it is possible to observe the agreement between the numerical and analytical solutions (Fig. 7). In a similar analysis, excellent stability and convergence of the Lobatto orthogonal base to the analytical solution is observed. However, opposite behavior is obtained for the equidistant base (Fig. 8).

The relative error of the numerical results in relation to the analytical solution is given by the equation:

$$e(\widetilde{n}_J) = \left|\frac{n_j - \widetilde{n}_j}{n_j}\right| \tag{35}$$

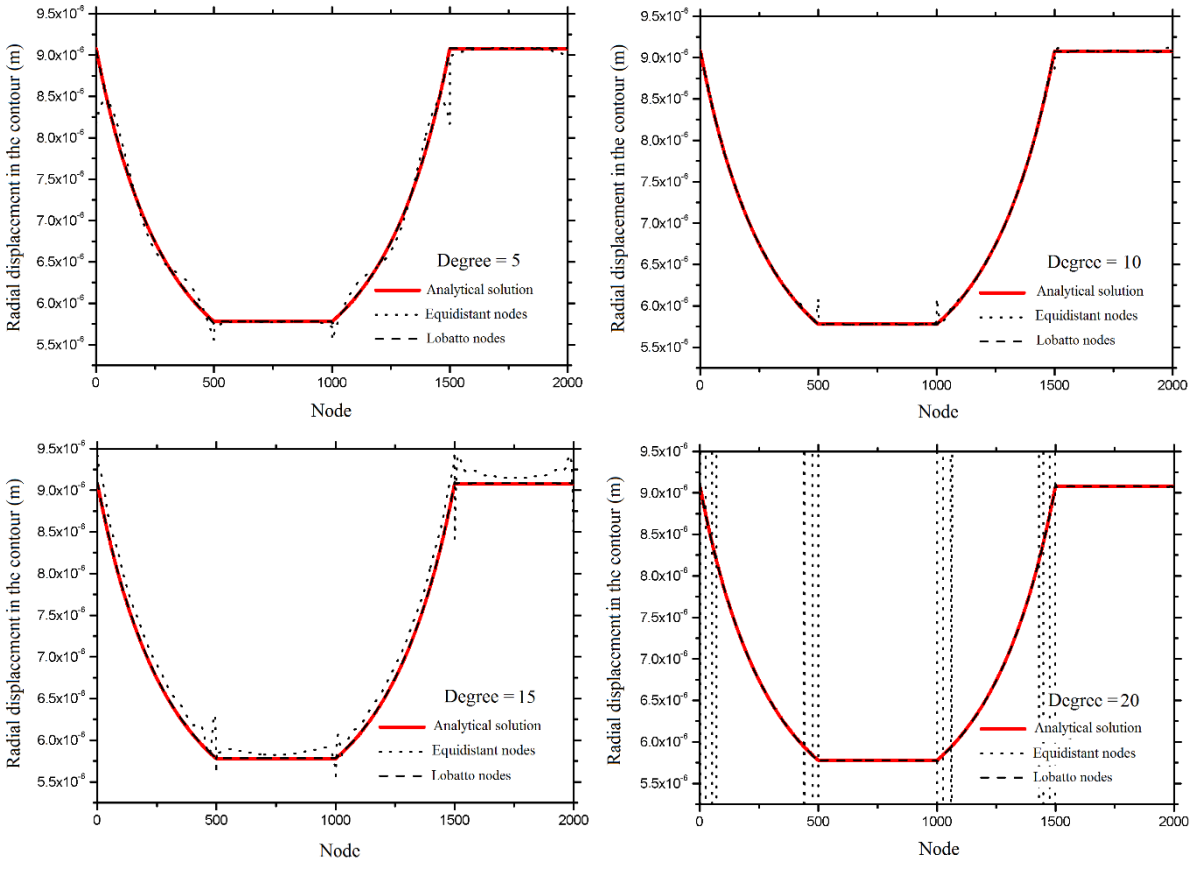

Figure 6. Radial displacement on the contour points

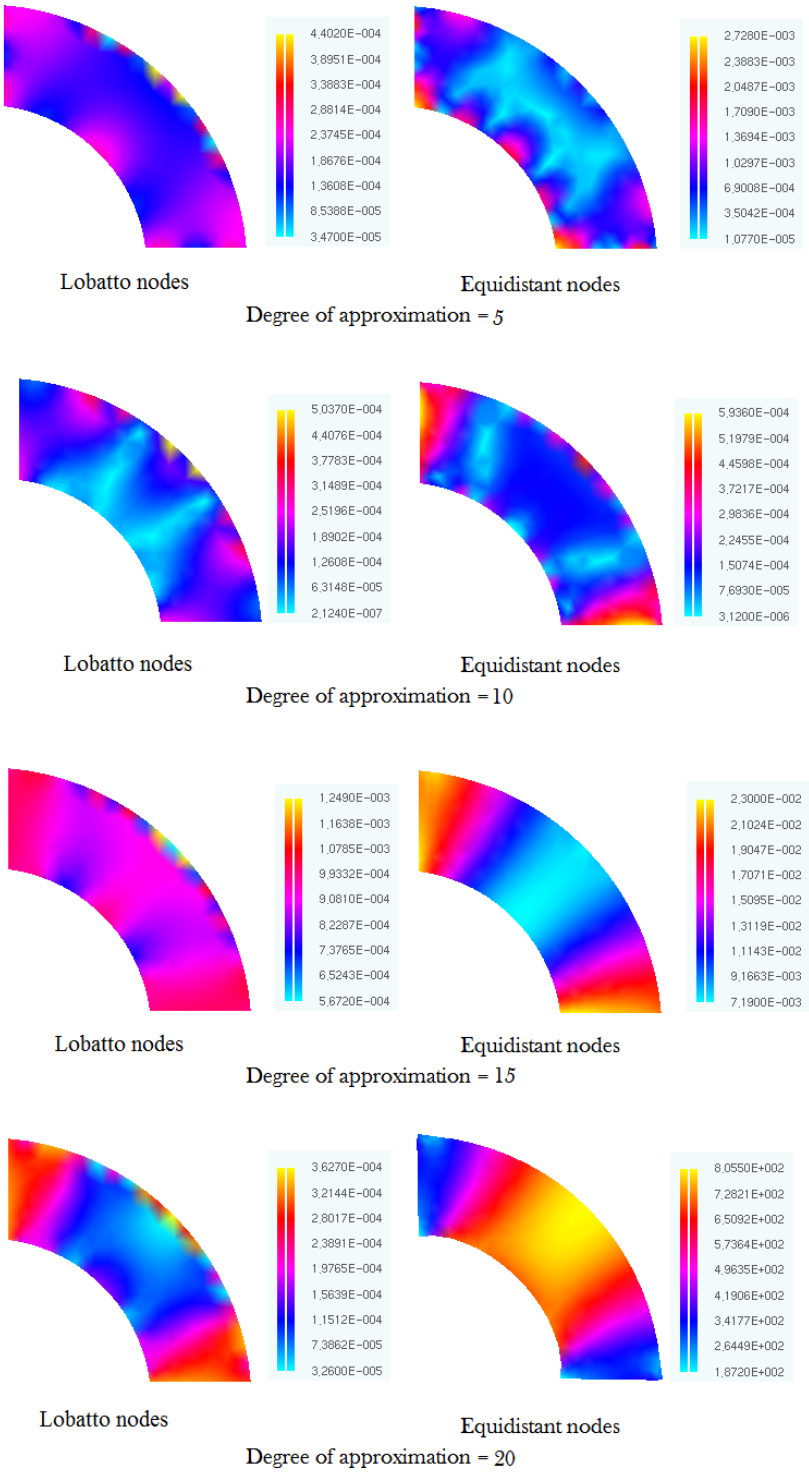

Figure 7. Relative error: displacement field in the domain.

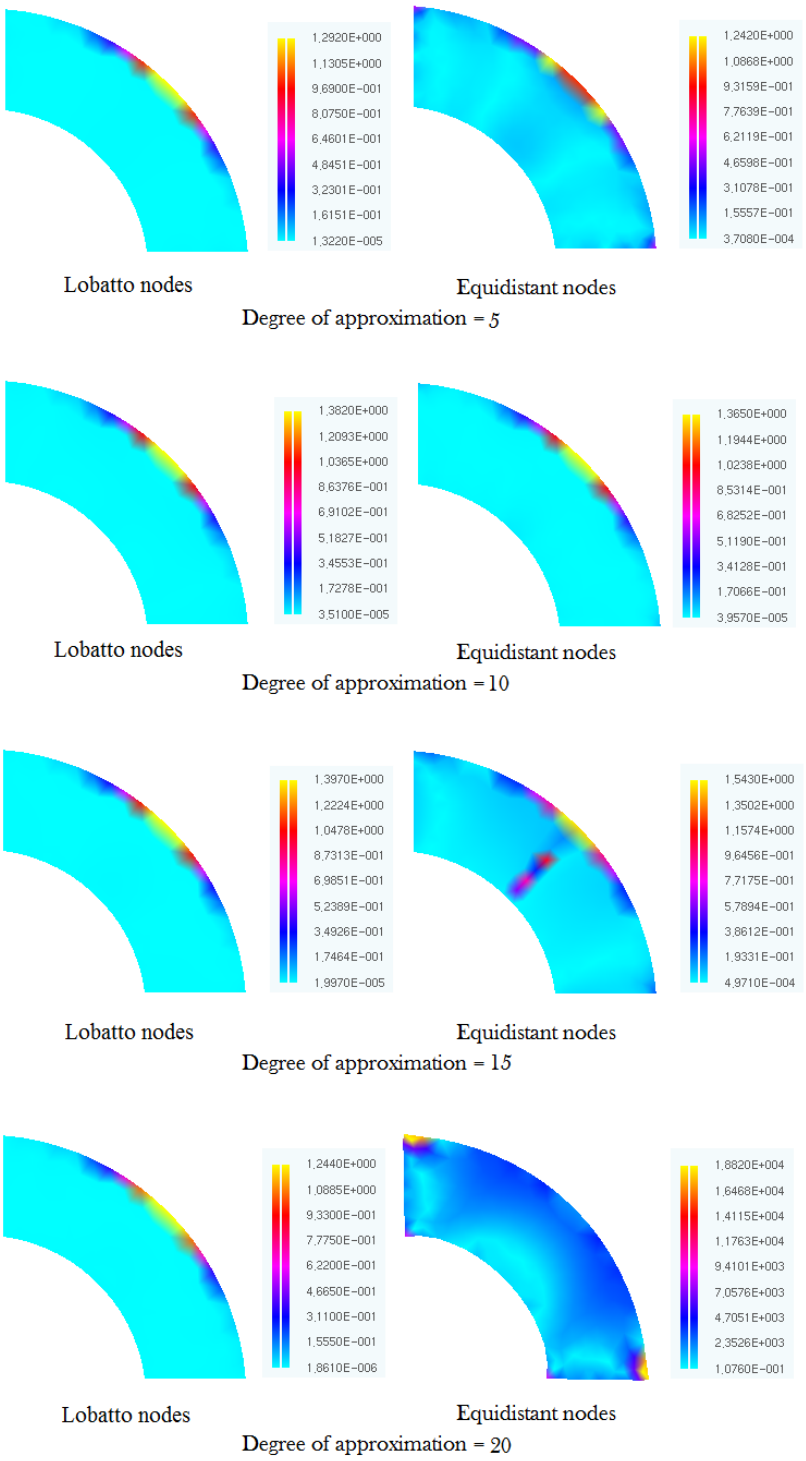

Figure 8. Relative error: stress field in the domain.

5 CONCLUSIONS

Based on presented data, it is verified that the the interpolation functions is very sensitive and depends on the position of the collocation points in the dimensionless space. To quantify this dependence, the Lebesgue constant and the condition number of the generalized Vandermond matrix were used.

According to the data presented in Fig (6 - 8), it was possible to verify the superiority of the interpolation for Lobatto nodal base of high order when compared with the equidistant nodal base for the elastostatic problems by BEM. Thus, it can be inferred that the use of high order Lobatto base provides stability and convergence and its use is recommended when it is desired to use any order approximations.

ACKNOWLEDGEMENTS

The authors thank COPES-UFS (Research Coordination of UFS) for granting a scientific scholarship.

REFERENCES

Aliabadi, M. H,. 2002. *The boundary element method: applications in solids and structures*. v. 2. Ed. Wiley.

Beer, G; Smith, I; Duenser, C., 2008. *The Boundary Element Method with Programming: For Engineers and Scientists*. Ed. Springer.

Brebbia, C. A., 1978. *The boundary element method for engineers*. London: Pentech Press.

Chen, Y. J., He, H. Y., Zhang, S. L., 2013. *A new algebra interpolation polynomial without*

Runge phenomenon. Applied Mechanics and Materilas, n. 303-306, pp. 1085-1088.

Franco, N. M. B., 2006. *Cálculo Numérico*. Ed. Pearson Prentice Hall.

Gao, X. W., 2010. *An effective method for numerical evaluation of general 2D and 3D high order singular boundary integrals. Computer methods in applied mechanics and engineering*, n. 199, pp. 2856–2864.

Karniadakis G. E., Sherwin S. J., 1999. *Spectral/hp element method for CFD*. Oxford: Oxford University Press.

Pozrikidis, C., 2005. *Introduction to Finite and Spectral Element Methods using MATLAB*. Chapman & Hall/CRC.

Pozrikidis, C., 1992. *Boundary integral and singularity methods for linearized viscous flow.Cambridge*. Cambridge University Press.

Rocha, F. C; Kzam, A. K. L; Coda, H. B., 2013. Análise das aproximações *de alta ordem por meio da interpolação espectral aplicados ao MEC potencial*. XXXIV CILAMCE, Pirenópolis.